Original Research

Quantification of Absolute Fat Mass Using an Adipose Tissue Reference Signal Model

Houchun H. Hu, PhD,* and Krishna S. Nayak, PhD

Purpose: To develop a method for quantifying absolute fat mass, and to demonstrate its feasibility in phantoms and in ex vivo swine specimens at 3 Tesla.

Materials and Methods: Chemical-shift-based fat-water decomposition was used to first reconstruct fat-only images. Our proposed model used a reference signal from fat in pure adipose tissue to calibrate and normalize the fat signal intensities from the fat-only images. Fat mass was subsequently computed on a voxel-by-voxel basis and summed across each sample. Feasibility of the model was tested in six ex vivo swine samples containing varying mixtures of fat (adipose) and lean tissues. The samples were imaged using 1.5-mm isotropic voxels and a single-channel birdcage head coil at 3 Tesla. Lipid assay was independently performed to determine fat mass, and served as the comparison standard.

Results: Absolute fat mass values (in grams) derived by our proposed model were in excellent agreement with lipid assay results, with a 5% to 7% difference ($r > 0.99$; $P < 0.001$).

Conclusion: Preliminary results in ex vivo swine samples demonstrated the feasibility of computing absolute fat mass as a quantitative endpoint using chemical-shift fat-water MRI with a signal model based on reference fat from pure adipose tissue.

Key Words: fat quantification; absolute fat mass; internal fat reference; adipose tissue reference; fat-water imaging; IDEAL
J. Magn. Reson. Imaging 2008;28:1483–1491.

OBESITY IS A GROWING EPIDEMIC that affects children and adults in the United States. Increased health risks include cardiovascular, endocrine, and metabolic diseases, which have been linked to fat accumulation in adipose tissue, skeletal muscles, and organs (ectopic fat) (1,2). Noninvasive assessment of fat distribution has become an important component in obesity research and preventive medicine, and accurate quantitative estimates of fat are sought as biomarkers for disease stratification.

Several methods are available for estimating body fat content (3). Anthropometric indices, hydrodensitometry, and air displacement plethysmography estimate *total percent body fat* with predictive equations. Bioelectric impedance analysis (BIA) and dual-energy X-ray absorptiometry (DXA) provide quantitative endpoints of total and regional body *fat mass*, and are the predominant methods used in obesity studies. However, BIA and DXA can not differentiate abdominal adipose tissue from ectopic fat. Fat quantification using computed tomography (4) and MRI (5) have recently gained popularity. Their three-dimensional (3D) image volumes and high spatial resolution can highlight fat distributions within the abdomen. MRI's flexible signal contrast can further identify fat infiltration in organs and muscles, and its lack of ionizing radiation is suitable for studying obesity in young cohorts.

One common MRI method uses T1-weighting to distinguish adipose from lean tissue (5). Quantification involves identifying "fat" voxels with a binary signal intensity histogram threshold. After image segmentation of the subcutaneous and visceral adipose tissue compartments, summation of voxels yields a *volume of adipose tissue* as the quantitative endpoint. This approach estimates adipose tissue, which also contains water, carbohydrate, and proteins in addition to fat (triglycerides). An alternative using spectrally selective radiofrequency (RF) pulses to excite fat protons was recently described (6), and a similar histogram procedure was used to quantify *fat volume* instead of adipose tissue volume. Both the T1 and spectrally selective RF methods assign each reconstructed voxel as either "fat" or "nonfat," or assumptions regarding partial volume are made (6). While quantitative errors due to partial volume are minimal for the well-delineated subcutaneous adipose tissue, they can be significant within the visceral compartment and in ectopic fat where patterns of heterogeneous fat distribution are probable (7). Consequently, neither method has been extended to quantify nonuniform and diffusely distributed ectopic fat.

Magnetic Resonance Engineering Laboratory, Ming Hsieh Department of Electrical Engineering, University of Southern California, Los Angeles, California.

Contract grant sponsor: NCI Centers for Transdisciplinary Research on Energetics and Cancer (TREC) ; Contract grant number: U54 CA 116848).

*Address reprint requests to: H.H.H., University of Southern California, Ming Hsieh Department of Electrical Engineering, 3740 McClintock Avenue, EEB 408, Los Angeles, CA. 90089-2564. E-mail: houchunh@usc.edu

Received March 12, 2008; Accepted August 21, 2008.
DOI 10.1002/jmri.21603
Published online in Wiley InterScience (www.interscience.wiley.com).

Chemical-shift MR, such as ^{1}H spectroscopy (8), in- and opposed-phase imaging (9), and generalized multipoint fat-water separation methods such as Iterative Decomposition with Echo Asymmetry and Least squares estimation—IDEAL (10), have been used to quantify ectopic fat in the study of liver steatosis (11,12) and in muscles (13). A relative *fat-water signal fraction* is typically reported as the quantitative endpoint, in spectroscopy as the ratio of areas under the fat and water spectra, and in the imaging methods as a fraction of the fat and water signal intensities. Because it is computed as a voxel-by-voxel ratio, one benefit of the signal fraction is that receiver coil sensitivities and RF transmit nonuniformities are approximately cancelled. Two works have shown that considerations of imaging parameters and data reconstruction steps are needed to further reduce T1 relaxation and noise bias in computing the fat-water signal fraction (14,15). In livers where high levels of iron may be present, T2* must also be included in the IDEAL algorithm (16). A recent study demonstrated the IDEAL fat-water signal fraction as a promising biomarker for fatty liver diseases (17).

In this work, we formulate an approach to compute *absolute fat mass* by combining IDEAL with a reference fat signal from pure adipose tissue. As we will demonstrate, our desired quantitative endpoint is the estimation of fat in absolute units of mass (e.g. grams). We selected IDEAL as the basis of our experiments due to the technique's robust performance in the presence of B0 off-resonance (10,18) and its ability to distinguish fat and water on a voxel-by-voxel basis. Experiments are performed in phantoms and ex vivo swine specimens to test feasibility. In the ex vivo study, MRI results are compared against gold-standard lipid assay.

MATERIALS AND METHODS

Theory

Let S_F and S_W denote the decomposed fat and water signals in a voxel $\bar{r}$, respectively, after IDEAL spoiled gradient echo (SPGR) reconstruction (10). The fat-water signal fraction (Eq. [1]) can suffer from T1 bias between fat and water protons. Small flip angles or T1-mapping approaches have been suggested to mitigate this T1 effect (14,15), such that the fraction accurately reflects the total number of fat (N_F) to water (N_W) protons in voxel $\bar{r}$.

$$\text{fat-water signal fraction}\,(\bar{r}) = \frac{S_F(\bar{r})}{S_F(\bar{r}) + S_w(\bar{r})} \equiv \frac{N_F(\bar{r})}{N_F(\bar{r}) + N_w(\bar{r})} \quad [1]$$

Without knowledge of the relative proton and mass densities of the voxel's underlying fat and lean (water) constituents, the fat-water signal fraction can not be converted to a fat-water volume (or mass) fraction. Although the chemical properties and mass densities of human fat and tissues are known (19–23), slight regional variations across the abdomen and possibly as a function of disease state can complicate consistent interpretations of the fat-water signal fraction. Nonetheless, several investigators have adopted specific proton-density conversion factors that extend the fat-water signal fraction to a fat-water volume fraction (8,11,24).

As an alternative to the fat-water signal fraction, we propose a *fat-only signal fraction* that does not involve the potentially confounding S_W term in Eq. [1]. This new ratio (Eq. [2]) normalizes the fat signal (S_F) in each voxel by an internal reference $S_{reference}$, where $S_{reference}$ denotes the IDEAL-reconstructed fat signal in a same-sized voxel from nearby *pure fat*. In the upcoming ex vivo study, our estimate of $S_{reference}$ comes specifically from pure fat in adipose tissue within the samples of interest.

$$\text{fat-only signal fraction}\,(\bar{r}) = \frac{S_F(\bar{r})}{S_{reference}} \quad [2]$$

Because both numerator and denominator values originate from fat (free fatty acids, triglycerides), the proposed ratio is likely less susceptible to proton and mass density variations than the fat-water signal fraction. Accordingly, we anticipate the fat-only signal fraction to more accurately reflect the true underlying fat content in each voxel without the need of fat-water conversion factors.

The fat-only signal fraction provides a path to compute absolute fat mass m (Eq. [3]) by multiplication with two constants, the voxel volume (v) and the fat mass density (ρ_F).

$$m(\bar{r}) = \left(\frac{S_F(\bar{r})}{S_{reference}}\right) \cdot v \cdot \rho_F \quad [3]$$

Eq. [3] is the central emphasis of this work as it estimates absolute fat mass on a voxel-by-voxel basis. Because v and ρ_F are scalar constants, errors in the quantification of m will depend on accurate signal intensities of S_F and $S_{reference}$. Although multiplication by v and ρ_F is required to explicitly obtain mass, the fat-only signal fraction itself is expected to vary linearly as a function of fat mass. While independent of the water signal that originally motivated investigations of T1 bias, there remains a possibility that the fat-only signal fraction (Eq. [2]) is also susceptible to T1 influence, in this case between S_F (fat in mixture) and $S_{reference}$ (pure fat).

In its present form, our proposed fat mass quantification model is not sufficient for application in human abdominal MRI, particularly at high field strengths (>1.5 Tesla [T]) where dielectric resonances and shorter RF wavelengths cause subject-dependent signal intensity modulations. The main concern is the model's sensitivity toward signal intensity shading generated by nonuniform RF transmit ($B1^+$) and receive ($B1^-$) fields. Because the reference fat signal $S_{reference}$ originates from separate voxels than S_F, $B1^{\pm}$ effects are consequently not removed in Eq. [2]. Incorrect fat-only signal fractions will result if significant B1 nonuniformity is uncompensated. Rapid and accurate mapping of $B1^{\pm}$ variations within the abdomen is challenging, and associated development of signal models using the principle of reciprocity to compensate $B1^{\pm}$ effects before quantitative analysis remain an active and ongoing area of research (25). Accordingly, we have limited the

scope of this work to focus on demonstrating the feasibility of computing absolute fat mass. We have attempted to minimize RF-induced signal variations by using a single-channel birdcage head coil in all experiments. B1 compensation was not explicitly considered in data processing. To justify B1 uniformity of the head coil at 3T, a signal intensity histogram of $S_{reference}$ from a large region ($>10^5$ voxels) of homogeneous pure adipose tissue and corresponding $B1^+$ flip angle distributions are presented in the Results section.

All experiments were performed on a 3T scanner (General Electric Healthcare, Waukesha, Wisconsin) with phantoms and ex vivo samples at room temperature. IDEAL echo times (TE) were selected to maximize signal-to-noise ratio (SNR), such that water and off-resonant spins of interest were separated by a phase of $\pm\pi/2$, $\pm 7\pi/6$, and $\pm 11\pi/6$, respectively (26), at the center of each corresponding echo.

Phantom Experiments

Eleven bottles containing 0 to 100% volume fraction of acetone (Alfa Aesar, Ward Hill, MA) and un-doped water were prepared in 10% increments (see Fig. 1). Acetone was used for convenience due to its complete miscibility with water. The purpose of the experiment was to demonstrate (a) potential T1 bias in Eq. [2], and (b) that normalization by an appropriate reference standard (pure acetone) can accurately reflect the true underlying content and provide a means of computing absolute mass. True volume and mass of acetone and water in each mixture were known. Acetone's mass density was determined as 0.78 g/mL and agreed with the manufacturer. Relative to water, acetone has a proton density of 0.73. Unlike fat, acetone has a single spectral peak, at approximately −2.3 parts per million (ppm) from the water peak. The phantom experiment was intended solely as a proof of concepts for the proposed quantification model described in Eqs. [2] and [3], and was not intended to characterize the more complex multi-spectra behavior of fat in vivo (27). The bottles were placed in a bowl filled with additional water.

Let $\bar{S}_A$ and $\bar{S}_W$ denote the mean signal intensities of IDEAL-reconstructed acetone and water in each mixture, respectively. Pure (100%) acetone provided an estimate of $S_{reference} = \bar{S}_{A(pure)}$. A 3D SPGR pulse sequence in conjunction with a T1-mapping approach (Driven Equilibrium Single Pulse Observation of T1—DESPOT1) (28) was used. Parameters were: repetition time (TR) = 70 ms, TEs = (1.9, 2.9, 4.0) ms, α = (5, 10, 20, 30, 40)°, bandwidth (BW) = ±125 kHz, field-of-view (FOV) = 20 cm, slice = 3 mm, 128 × 128 matrix. After IDEAL reconstruction, the T1 of acetone and water were extrapolated by curve-fitting the steady-state $\bar{S}_A$ and $\bar{S}_W$ SPGR signals from the separated component images. Next, the phantom was imaged again with TR = 6 ms and $\alpha = 3°$ (all other parameters same as before). A flip angle of 3° was used to minimize T1 bias between $\bar{S}_A$ and $\bar{S}_{A(pure)}$ (see Fig. 1). The acetone–water signal-fraction for each mixture was computed as $\bar{S}_A/(\bar{S}_A + \bar{S}_W)$, along with the proposed signal normalization $\bar{S}_A/\bar{S}_{A(pure)}$. The acetone–water mass fraction was also calculated. Lastly, the absolute mass of acetone in each mixture was determined from $\bar{S}_A/\bar{S}_{A(pure)}$ and Eq. 3 and summing across voxels encompassing each bottle.

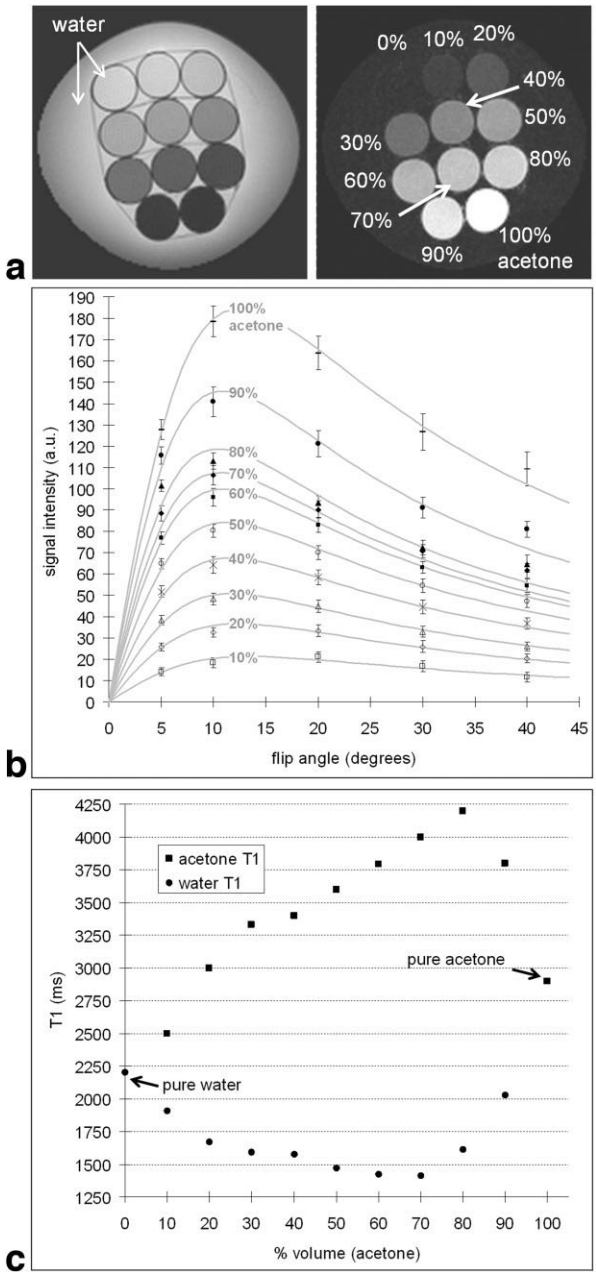

Figure 1. a: IDEAL-reconstructed water (left) and acetone (right) component images from the mixture phantom, shown from a data set acquired with a 5° flip angle. Note uniform separation of the water and acetone constituents. **b:** IDEAL-reconstructed mean acetone signal intensities are plotted as a function of flip angle for mixtures with acetone volume fractions between 10% and 100%. Corresponding fitted curves of the steady-state SPGR signal are also shown. **c:** Extrapolated T1 values for acetone and water, plotted as a function of acetone volume fraction.

A second phantom experiment, similar to the acetone–water setup, was performed using lard (unrendered pork fat, Farmer John, Los Angeles, CA) and lean bovine tissue obtained from a local market. The lean tissue contained no visible pockets of fat. Seven indi-

vidual mixtures consisting of known lard and lean tissue masses were homogeneously blended and prepared (see Fig. 3). All experimental steps were identical to the acetone–water experiment, with the exception of TEs = (2.0, 2.8, 3.5) ms tailored for fat-water separation. Subsequent data processing steps were also similar. In addition to DESPOT1, which separately estimated the T1 of lard and lean tissue components *within* each mixture, we also performed inversion-recovery spin-echo (IRSE, TR = 4 s, inversion time = 50–800 ms, TE = 8 ms, 10 mm slice, BW = ±16 kHz) measurements to ascertain the T1 of each bottle's mixed content. Bottles of pure lard and pure vegetable (corn) oil served as reference standards in computing the fat-only signal fractions.

Ex Vivo Swine Experiments

MRI

To explicitly compute fat mass, knowledge of ρ_F is required. A pilot experiment was performed to determine ρ_F in swine. In the present framework, ρ_F specifically denotes the mass density of fat in reference adipose tissue. Three samples of pure swine adipose tissue (40 to 76 grams) were imaged (TR = 5 ms, TEs = [2.0, 2.8, and 3.5] ms, $\alpha = 5°$, BW = ±62.5 kHz, FOV = 20 cm, slice thickness = 2.5 mm, 192 × 192 matrix). The number of voxels containing each sample was identified and multiplied by v to determine sample volume. Fat mass was separately determined with lipid assay (described later), and ρ_F was calculated. Next, two sets of data were collected from six additional swine specimens (45 to 615 grams) containing unknown mixtures of fat and lean tissues. *Spatial Resolution*: each sample was imaged with 3D SPGR: TR = 6.5 ms, TEs = (2.0, 2.8, and 3.5) ms, $\alpha = 5°$, BW = ±125 kHz, FOV = 28 cm, 192 × 192 sampling matrix, 1.5 mm isotropic resolution, six individual repetitions. To investigate variations in fat mass quantification due to voxel size, these data sets were down-sampled to 3 mm (samples 1–6) and 4 mm (samples 5 and 6) isotropic formats. *Flip Angle and T1 Bias*: samples 1–5 were again imaged with the above pulse sequence, but with a constant 3-mm isotropic voxel and α = (1, 3, 10, 20, and 30)°. The goal was to investigate the dependence of fat mass and the associated fat-only signal fraction on flip angle due to T1 bias and compare our findings with T1 results from the lard-tissue phantom experiment. After IDEAL reconstruction, where fat was modeled with a single −3.5 ppm chemical shift, an estimate of $S_{reference}$ was obtained from regions of homogeneous pure adipose tissue within each sample ($>10^3$ voxels). Each sample's fat mass was then computed by substituting ρ_F with the value derived from the pilot experiment, the appropriate voxel size v, and summing across relevant voxels.

Lipid Assay

All swine samples were independently analyzed for fat mass with lipid assay (29). The samples were weighed and placed in an oven at 60°C for desiccation. Samples were dried until constant weight, upon which loss in water mass was determined. The samples were then ground to powder, placed in cellulose extraction thimbles, and weighed. The thimbles were set in a Soxhlet apparatus, where multiple cycles of petroleum ether extraction were performed. Afterward, samples were allowed to dry, and reweighed to determine the loss in fat mass. Lipid assay is considered the benchmark for animal carcass analysis and is the method against which other body composition techniques are evaluated.

Transmit B1$^+$ Mapping

To assess RF transmit nonuniformity of the 3T single-channel head coil, measurements of actual flip angle ($B1^+$) distributions were made across sagittal and coronal slices in one of the large swine samples. The saturated double-angle method (SDAM) (30) was used (saturation recovery time = 600 ms, BW = ±16 kHz, FOV = 24 cm, 64 × 64 matrix, and slice thickness = 5 mm).

RESULTS

Phantom Experiments

Figure 1a shows decomposed water and acetone images from the phantom. Figure 1b plots the mean acetone signal $\bar{S}_A$ as a function flip angle for each mixture, along with fitted steady-state SPGR signal curves. Similar plots were obtained for the water component $\bar{S}_W$ (not shown). Extrapolated T1 values of acetone and water are summarized in Figure 1c. Note that both the T1 of acetone and water in mixture vary by as much as 40% of their corresponding pure T1 values. The maximum T1 deviation for acetone and water was observed in the 80% and 70% mixtures, respectively. In particular, note that $T1_{acetone}$ approaches that of pure water (2200 ms) as the volume fraction decreases toward pure water, while $T1_{water}$ approaches that of pure acetone (2900 ms) as the volume fraction increases toward pure acetone. This corroborates our speculation that T1 bias remains in the proposed signal fraction (Eq. [2]).

Figure 2 illustrates the disparity between the acetone–water signal fraction (ordinate) and the true acetone volume fraction (abscissa). The acetone–water signal fraction (○) deviates from the identity line (gray, slope = 1) for 20 to 80% mixtures. A similar trend is observed for the acetone–water mass fraction (×). These disagreements are expected, and are caused by differences in the proton and mass densities of acetone and water. In contrast, the $\bar{S}_A/\bar{S}_{A(pure)}$ acetone-only signal fraction (●) exhibits strong linear correlation with the underlying true acetone volume fraction (black line, slope = 0.97). Note the 4% bias for the 0% (pure water) data point due to the Rician noise behavior of magnitude data (14). Table 1 tabulates the true acetone mass measured during phantom preparation versus MRI estimates, showing good agreement with a maximum difference of 4.8%.

Figure 3a shows a photograph of the homogeneously blended lard and lean bovine tissue mixtures, along with water and fat component images. Figure 3b plots the extrapolated T1 of lard (circle) and lean tissue (square) for each mixture. T1 values of pure lard (253 ms) and pure lean tissue (680 ms) appear reasonable and are in good agreement with values obtained by

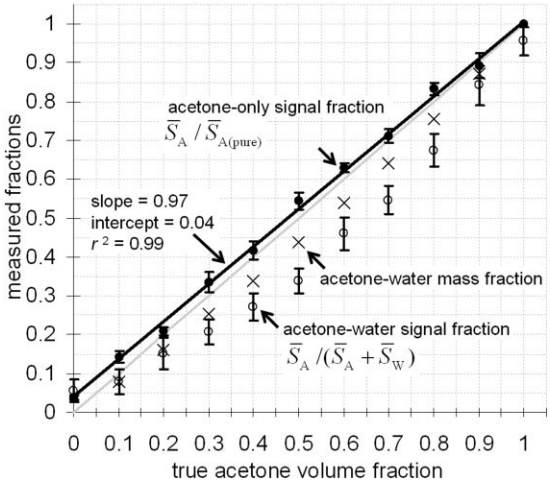

Figure 2. Results from phantom experiment. For mixtures with intermediate proportions of 20% to 80%, both the acetone–water signal fraction (○) and the acetone–water mass fraction (×) deviate from the true acetone-volume fraction (gray line: identity) due to differences in acetone and water proton and mass densities. The proposed acetone-only signal fraction (●) exhibits strong linear correlation (black line).

IRSE (×). Note that $T1_{lean\ tissue}$ and $T1_{lard}$ both vary as a function of lard content, similar to the findings of Poon et al (8), and that the T1 of each mixture as determined by IRSE falls in between the T1 values of the individual components. Figure 3c plots the sum of the fat-only signal fractions of each phantom bottle. The ordinate in Figure 3c represents the sum of the term in parenthesis in Eq. 3. The scalars v and ρ_F have not been applied in this case. As expected, the fat-only signal fraction tracks linearly with the true underlying lard mass, regardless of whether pure lard (black, $S_{reference} = S_{pure\ lard}$) or pure corn oil (gray, $S_{reference} = S_{vegetable\ oil}$) was used to provide the reference fat signal (Pearson cross correlation $r > 0.95$). The difference between the two slopes reflects the difference in proton density between the lard and oil references. By taking the known lard masses, the corresponding fat-only signal fractions computed using $S_{pure\ lard}$, and adjusting for v, the average mass density of lard was retrospectively estimated to be a reasonable 0.91 g/mL.

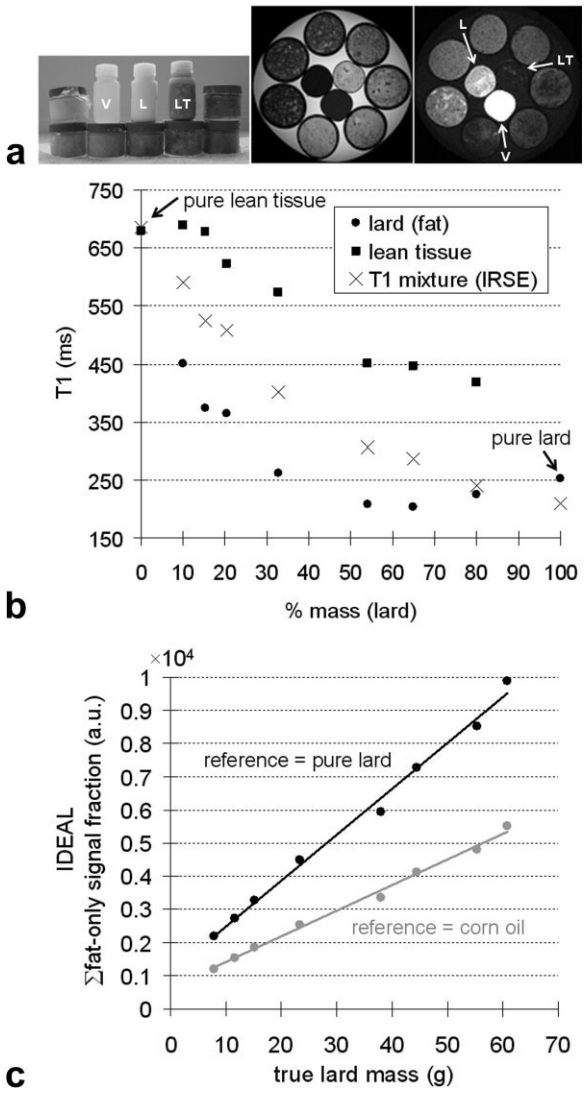

Figure 3. a: Photograph (left) and IDEAL reconstructed water (middle) and fat (right) images of lard and lean bovine tissue mixtures. Whiter appearance in the photograph reflects greater lard content. *V* = pure vegetable oil, *L* = pure lard, *LT* = pure lean tissue. **b:** T1 values of lard and lean tissue as determined by DESPOT1. IRSE measurement of each mixture's T1 is also shown. **c:** Plot of fat-only signal fractions without scaling by voxel size and mass density, showing strong linear correlation with underlying lard mass regardless of the fat reference signal used (black, pure lard; gray, pure vegetable oil).

Table 1
Results From Phantom Experiment Comparing True Acetone Mass Measured a Priori Versus MRI-Estimated Acetone Mass

acetone (% volume)	true acetone mass (g)	estimated acetone mass (g)	mean % difference
10	2.3	2.4 ± 0.36	4.2
20	4.6	4.7 ± 0.48	2.7
30	7.1	6.8 ± 0.32	−4.8
40	9.2	9.6 ± 0.75	4.6
50	11.7	11.9 ± 0.68	1.7
60	14.0	13.7 ± 0.55	−2.3
70	16.2	16.3 ± 0.29	0.5
80	18.5	18.4 ± 0.49	−0.5
90	20.7	20.1 ± 0.39	−3.0
100	23	23.7 ± 0.84	2.9

Ex Vivo Swine Experiments

From the pilot study, ρ_F in swine was estimated between 0.79 and 0.8 g/mL, which agrees with the range reported in literature (31,32). Figure 4 shows photos and single slice IDEAL images of samples 3, 4, and 6. Arrows denote regions of homogeneous pure adipose tissues that were used to estimate $S_{reference}$. Figure 5a plots a correlation between lipid assay fat mass and those derived by MRI with 1.5-mm isotropic voxel data. The

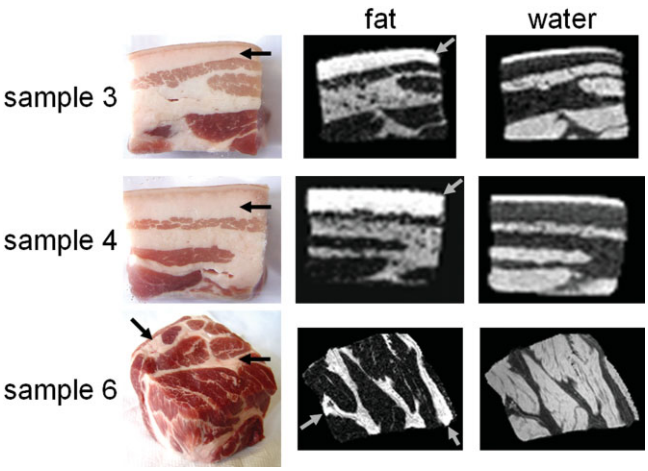

Figure 4. Representative photos and single slice fat- and water-component images of samples 3, 4, and 6 (flip angle = 5°, 1.5-mm voxel). Arrows highlight homogeneous adipose tissue regions that are used to estimate the internal reference fat signal, $S_{reference}$.

inset is an enlargement of the gray shaded region for samples 1 through 4. The data points reflect each sample's fat mass from six MRI data repetitions. The regression line (black) has a slope of 1.07 relative to the identity line (gray). Figure 5b shows results from the simulated 3 mm isotropic voxel data with similar correlation. Repeatability of MRI-derived fat mass results was very high, and only a 1% to 4% variation was observed. The mean percent difference between MRI and lipid assay was 6.8% (range: 0.5% to 13.8%) for the 1.5 mm data set, 6.3% (range: 2.0% to 10.3%) for the 3 mm data set, and 8.8% (range: 5.6% to 12.0%) for the 4 mm data set (samples 5 and 6 only). Overall, a strong agreement between the proposed fat mass quantification model and lipid assay was achieved ($r > 0.99$; $P < 0.001$).

Figure 6 plots the mean MRI fat mass as a function of flip angle for samples 1 through 5. Variation in fat mass across six data repetitions was less than 2% and the corresponding indiscernible error bars have been excluded. Note the discontinuity along the vertical axis and the small interval size of 2 grams. Fat mass variation across the range of flip angles was 6.5%, 2.7%, 2.1%, 5.6%, and 6.4% for samples 1 through 5, respectively. Linear regression of the computed fat mass versus the flip angle range (T1 dependence) yielded insignificant slopes (< 0.05, not shown), which indicates no apparent dependence between the two quantities. In contrast to results from the phantom experiments, Figure 6 suggests minimal T1 differences between S_F (fat in mixture) and $S_{reference}$ (pure fat in adipose tissue) within the ex vivo swine samples considered in this work. Possible reasons for this disparity are elaborated in Discussion.

Figure 7a,b illustrate histograms of the $B1^+$ distribution across four coronal and sagittal slices of a large swine sample, respectively. The abscissa represents the range of true flip angles computed by SDAM, while the nominal flip angle prescribed at the scanner console was 60°. The mean, standard deviation, and coefficient of variation of the $B1^+$ distribution were 61.7°, 5.9°, and 9.6% (Fig. 7a), and 59.9°, 5.6°, and 9.4% (Fig. 7b). Figure 7c illustrates a normalized histogram of the internal fat reference from nearly 144,500 voxels of pure homogeneous adipose tissue, which has a coefficient of variation of 13.5%.

DISCUSSION

We have described a quantification model to compute absolute fat mass based on a combination of multipoint chemical shift fat-water MRI and a fat reference signal. In the ex vivo experiment, the reference signal originated from pure fat in pure adipose tissue. We have demonstrated feasibility by first computing a fat-only signal fraction that does not involve the water component, followed by adjustments for voxel size and fat

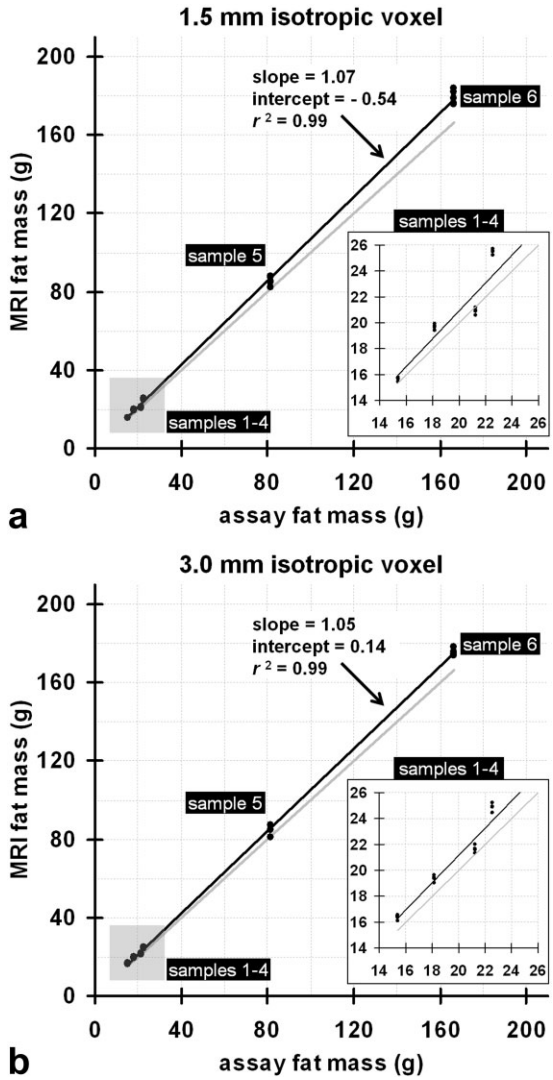

Figure 5. a,b: Correlation plots between lipid assay and MRI-derived fat mass results for (a) 1.5 mm and (b) simulated 3-mm isotropic voxels. Inset shows enlargement of gray shaded region for samples 1 through 4. Gray line: identity. Black line: linear regression. Not all data points are visible due to the strong repeatability of the MRI results, with only 1–4% variation across six repeated measurements.

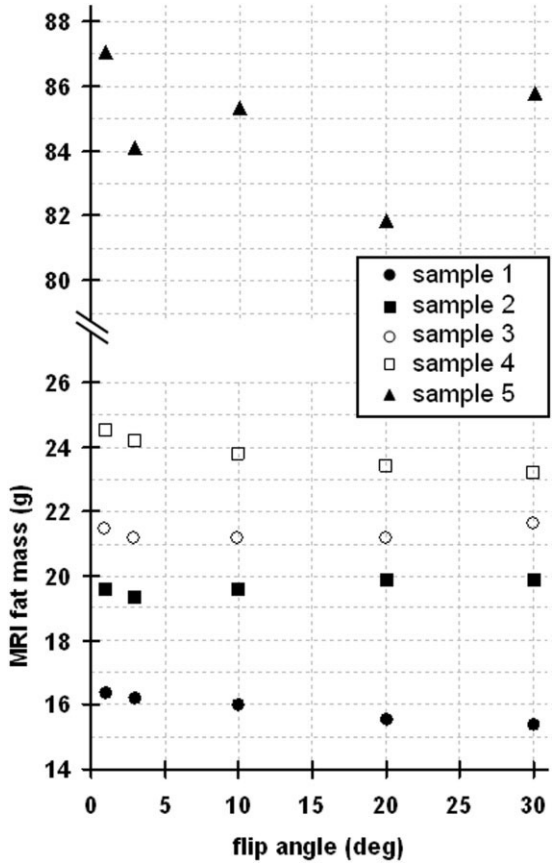

Figure 6. Plot of mean fat mass derived from MRI using a 3-mm isotropic voxel as a function of imaging flip angle. Linear regression (not shown) yields slopes of less than 0.05, suggesting no apparent dependence of the fat mass estimate and related fat-only signal fraction on flip angle between 1° and 30°. Note vertical axis discontinuity and small 2-gram intervals.

mass density. Preliminary results showed good agreement between lipid assay and MRI, with approximately a 5% to 7% difference. For 1.5 to 4 mm isotropic voxels, there appeared to be no evident trend supporting greater accuracy of fat mass estimates with higher spatial resolution. This is largely due to the robustness of IDEAL in decomposing fat and water component signals within such nominally sized voxels. The use of larger voxels should be advantageous for in vivo fat quantification, where rapid abdominal imaging during breath-holds is essential.

Results from the acetone–water and lard–lean tissue phantom experiments suggested possible T1 bias in our proposed signal fraction (Eq. [2]). On the contrary, this T1 bias was not observed in the ex vivo swine results. A possible explanation of this disparity is that in both phantom experiments, the constituents were uniformly mixed. For the acetone–water setup, both components were completely miscible. For the lard–lean tissue experiment, each mixture was homogeneously blended. Because the rate of T1 relaxation fundamentally depends on a match between the Larmor frequency and the molecular tumbling rate of the lattice, it is conceivable that varying proportions of uniformly mixed acetone–water and lard–lean tissue preparations established lattices that contributed to different tumbling rates and associated correlation times of the resident proton spins, thereby causing the T1 fluctuations observed in Figures 1c and 3b. In contrast, the swine samples used in this work contained discrete pockets of fat infiltration that had limited miscibility with the neighboring lean tissues. Consequently, it is plausible that the immediate lattice surrounding a lipid isochromat in a voxel containing both fat and lean components is almost entirely "fatty" and likely similar to the lattice within a voxel containing reference pure adipose tissue fat. Accordingly, the T1 of fat remains relatively unaltered. Despite these observations, T1 bias should remain a concern when quantifying ectopic fat in organs and intramuscular locations. In these regions, fat is indeed diffusely spread throughout the tissue medium, similar to the scenario modeled by the lard–lean tissue phantoms.

We have limited the scope of this work and performed experiments using a single-channel birdcage head coil

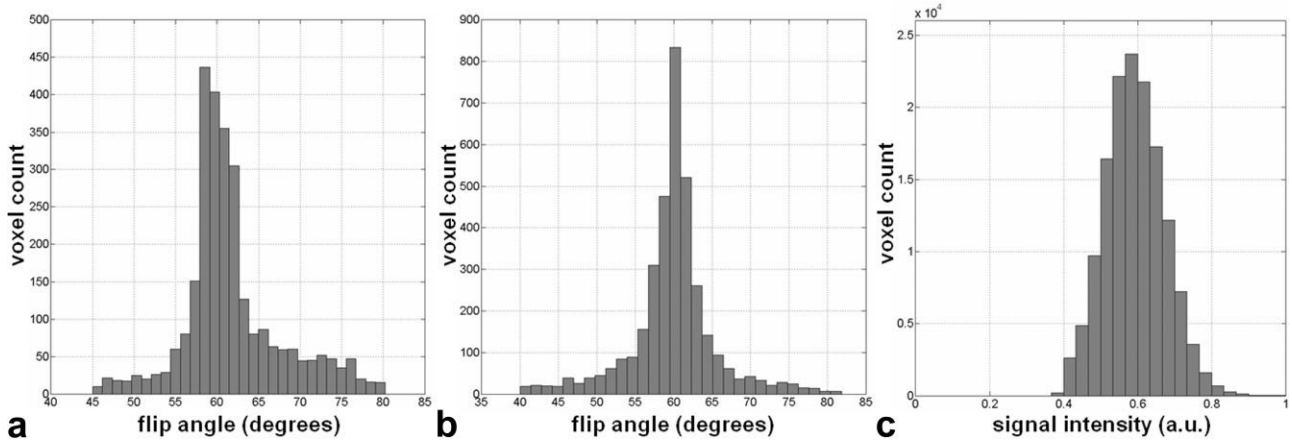

Figure 7. **a,b:** Histograms of the $B1^+$ (actual flip angle) distribution of the 3T transmit/receive single-channel bird cage head coil across coronal (a) and sagittal (b) slices of a large swine sample. The nominal (prescribed) flip angle was 60°. Mean, standard deviation, and coefficient of variation of the histograms are (a) 61.7°, 5.9°, and 9.6%, and (b) 59.9°, 5.6°, and 9.4%. **c:** Histogram of the reference fat signal intensity, $S_{reference}$, from nearly 144,500 voxels of pure adipose tissue. The corresponding coefficient of variation is 13.5%.

to minimize RF nonuniformity. Figure 7 summarized the relative homogeneity of the $B1^+$ transmit field of the head coil. The mean actual flip angle across the swine sample was within 1% to 2% of the nominal 60° value. A 13.5% coefficient of variation was measured in the reference fat signal intensity distribution. Considering the approximate 9% coefficient of variation that was measured in the corresponding $B1^+$ distribution, results in Figure 7 indicate that adipose tissue is in fact quite homogeneous. A primary challenge in the application of the proposed fat mass quantification model for abdominal imaging is the anticipated high levels of RF nonuniformity within the abdomen, particularly at 3T, due to increasing dielectric and wavelength effects. A compensation model that uses the low-flip-angle IDEAL approach and the reciprocity principle to mitigate signal intensity shading has been suggested and implemented with limited success (33). Passive approaches using dielectric cushions have also been reported (34). Further investigation of RF nonuniformity is warranted, and the ongoing development of both B1 mapping and compensation schemes should make the fat mass quantification approach for in vivo applications realizable, especially at 1.5T where RF nonuniformity is less severe.

For in vivo abdominal applications, a multi-coil phased array is typically used as the signal receiver for practical SNR benefits. The nonuniform $B1^-$ receive field of phased-array coils can be compensated (35). Similar to the measurement of coil sensitivity profiles in parallel imaging, the ratio of a pair of low resolution images acquired separately with the body coil and with the phased-array provides a *relative* receive map that is adequate for parallel image reconstruction and removal of signal intensity modulations imposed by the phased-array receivers. However, signal intensities of the resultant intermediate corrected image remain modulated by the *absolute* RF transmit and receive fields of the body coil. Although the former can be accounted for with techniques like SDAM, approaches to directly measure or estimate the latter in vivo remain an unmet need in MRI, especially at high B0 field strengths where magnitude equality between the $B1^+$ and $B1^-$ fields can no longer be assumed (36,37).

The large dimensions of the subcutaneous adipose tissue layer in obese patients should be adequate for estimating $S_{reference}$. One disadvantage of using anatomy-based references is that the morphology can change with time, especially in longitudinal studies where patients are undergoing interventions. Alternatively, fiducial samples of vegetable oil or homogenized lard, or even adipose tissue, can be used. However, temperature differences between the fiducials and the sample of interest should be considered, as spin polarization and chemical shift can vary accordingly. In theory, it is also not necessary for the internal or external reference fat signal to originate from pure adipose tissue. As data from the lard–lean tissue experiment alluded to, the use of different fat references simply adds additional scaling to the fat-only signal fraction. These scalar constants would need to be determined accordingly. The use of oil fiducials (38) and internal bone marrow fat (39) in skeletal muscle lipid quantification have been reported. For large-FOV abdominal imaging, the influence of gradient nonlinearity will also require compensation, because signal compaction at the edges of the warped FOV can lead to inaccurate estimates of S_F and $S_{reference}$.

Additional modifications can be integrated into the IDEAL algorithm to improve fat-water decomposition. Correction for short T2* is necessary at air-tissue interfaces and in livers with high iron levels (16). T2* relaxation was not considered in this work. Another issue is that animal fat is characterized by a multi-component spectrum (27). The original IDEAL algorithm modeled fat with a single spectral peak at a frequency offset of −3.5 ppm from water. This assumption only accounts for the majority of methylene ($-(CH_2)_n-$) and terminal methyl ($-CH_3$) protons in triglycerides. Olenific protons ($-HC=CH-$) have peaks that are closer to water, and α-protons ($-CH_2$-$CO-$, $-CH_2$-$HC=CH-$) have peaks that are midway between the main water and fat peaks. Under the simplified model, signals from these protons become ambiguous and are erroneously assigned to the water component. Although the amplitudes of these minority peaks are orders of magnitude smaller than the primary methylene and methyl peaks, their impact on fat quantification has been investigated with multi-fat-peak IDEAL (40). Multi-fat-peak IDEAL can be useful in determining correction factors if the chemical composition (proton density) of the fat reference is suspected to be significantly different from that of the fat to be quantified. The neglected minority fat peaks in single-fat-peak IDEAL are one potential source of error in the 5–7% disagreement between MRI and lipid assay results reported in this work.

The density of fat (ρ_F) is needed to explicitly reach a quantitative endpoint of absolute fat mass from the fat-only signal fraction. However, this parameter is treated simply as a scaling constant in Eq. [3] and may not be entirely necessary. As demonstrated in Figure 3c, the sum of the fat-only signal fraction across a sample is linearly correlated to the underlying absolute fat mass, and the degree of proportionality reflects the difference in proton density between the fat reference and the fat of interest. Our pilot experiment with pure adipose tissue samples yielded an estimate of ρ_F in reasonable agreement with literature, which typically assumes that adipose tissue has a mass density of 0.93 g/mL and is composed of 83% percent volume fat (31,32). However, it has been shown that although the mass density of most animal fats is fairly constant at approximately 0.91 g/mL (19), the mass density of fat in adipose tissue can vary significantly with age (21). This is largely due to changes in the volume percent composition of fat in adipose tissue. Extensions to quantify ectopic fat distributions will require ρ_F to reflect the mass density of triglycerides and free fatty acids outside of adipose tissue. Because data on the mass densities of human trunk tissues are available in the literature (20,22,23), it would be useful to perform animal biopsy studies to determine the average percent fat content in these tissues. In doing so, the associated fat mass density in these specific tissues can be estimated. Alternatively, direct measurement of in vivo ρ_F may be feasible using multiple fiducials with known densities as a calibration step, although differences in

proton density must still be considered and makes the approach challenging.

In conclusion, the feasibility of estimating absolute fat mass using IDEAL has been demonstrated. The technique requires further testing in organs and larger animal samples in conjunction with development of RF nonuniformity compensation. Despite its rapid development over the past 2 decades, MRI remains an untapped resource in body composition and obesity. The approach for quantifying absolute fat mass described herein remains to be validated as a useful biomarker for the assessment of fat distribution.

ACKNOWLEDGMENTS

The authors thank Maria S. Johnson, Ph.D., and Tim R. Nagy, Ph.D., from the University of Alabama at Birmingham for performing the lipid assays, and Michael I. Goran, Ph.D., and Hee-Won Kim, Ph.D., at the University of Southern California for helpful discussions on fat quantification and T1 relaxation, respectively.

REFERENCES

1. Goran MI, Gower BA. Relation between visceral fat and disease risk in children and adolescents. Am J Clin Nutr 1999;70:149S–156S.
2. Despres JP, Lemieux I. Abdominal obesity and metabolic syndrome. Nature 2006;444:881–887.
3. Ellis KJ. Human body composition: in vivo methods. Physiol Rev 2000;80:649–680.
4. Maurovich-Horvat P, Massaro J, Fox CS, Moselewski F, O'Donnell CJ, Hoffmann U. Comparison of anthropometric, area- and volume-based assessment of abdominal subcutaneous and visceral adipose tissue volumes using multi-detector computed tomography. Int J Obes (Lond) 2007;31:500–506.
5. Machann J, Thamer C, Schnoedt B, et al. Standardized assessment of whole body adipose tissue topography by MRI. J Magn Reson Imaging 2005;21:455–462.
6. Peng Q, McColl RW, Ding Y, Wang J, Chia JM, Weatherall PT. Automated method for accurate abdominal fat quantification on water-saturated magnetic resonance images. J Magn Reson Imaging 2007;26:738–746.
7. Peng Q, Zhou A, Ding Y, McColl RW, Weatherall PT. Visceral fat quantification on MRI: the impact of partial volume effects. In: Proceedings of the 16th Annual Meeting of ISMRM, Toronto, 2008. (abstract 3042).
8. Poon CS, Szumowski J, Plewes DB, Ashby P, Henkelman RM. Fat/water quantitation and differential relaxation time measurement using chemical shift imaging technique. Magn Reson Imaging 1989;7:369–382.
9. Hussain HK, Chenevert TL, Londy FJ, et al. Hepatic fat fraction: MR imaging for quantitative measurement and display—early experience. Radiology 2005;237:1048–1055.
10. Reeder SB, McKenzie CA, Pineda AR, et al. Water-fat separation with IDEAL gradient-echo imaging. J Magn Reson Imaging 2007; 25:644–652.
11. Longo R, Pollesello P, Ricci C, et al. Proton MR spectroscopy in quantitative in vivo determination of fat content in human liver steatosis. J Magn Reson Imaging 1995;5:281–285.
12. Kim H, Taksali SE, Dufour S, et al. Comparative MR study of hepatic fat quantification using single-voxel proton spectroscopy, two-point dixon and three-point IDEAL. Magn Reson Med 2008;59: 521–527.
13. Weis J, Johansson L, Ortiz-Nieto F, Ahlstrom H. Assessment of lipids in skeletal muscle by high-resolution spectroscopic imaging using fat as the internal standard: comparison with water referenced spectroscopy. Magn Reson Med 2008;59:1259–1265.
14. Liu CY, McKenzie CA, Yu H, Brittain JH, Reeder SB. Fat quantification with IDEAL gradient echo imaging: correction of bias from T1 and noise. Magn Reson Med 2007;58:354–364.
15. Bydder M, Yokoo T, Hamilton G, et al. Relaxation effects in the quantification of fat using gradient echo imaging. Magn Reson Imaging 2008;26:347–359.
16. Yu H, McKenzie CA, Shimakawa A, et al. Multiecho reconstruction for simultaneous water-fat decomposition and T2* estimation. J Magn Reson Imaging 2007;26:1153–1161.
17. Gard CA, Warner TF, Yu H, et al. Quantification of hepatic steatosis with MRI: validation in the Ob/ob mouse at 3T. In: Proceedings of the 16th Annual Meeting of ISMRM, Toronto, 2008. (abstract 707).
18. Bernard CP, Liney GP, Manton DJ, Turnbull LW, Langton CM. Comparison of fat quantification methods: a phantom study at 3.0T. J Magn Reson Imaging 2008;27:192–197.
19. Fidanza F, Keys A, Anderson JT. Density of body fat in man and other mammals. J Appl Physiol 1953;6:252–256.
20. Allen TH, Krzywicki HJ, Roberts JE. Density, fat, water and solids in freshly isolated tissues. J Appl Physiol 1959;14:1005–1008.
21. Baker GL. Human adipose tissue composition and age. Am J Clin Nutr 1969;22:829–835.
22. Huang HK, Wu SC. The evaluation of mass densities of human body in vivo from CT scans. Comput Biol Med 1976;6:337–343.
23. Erdmann WS, Gos T. Density of trunk tissues of young and medium age people. J Biomech 1990;23:945–947.
24. Wehrli FW, Hopkins JA, Hwang SN, Song HK, Snyder PJ, Haddad JG. Cross-sectional study of osteopenia with quantitative MR imaging and bone densitometry. Radiology 2000;217:527–538.
25. Hu HH, Sung K, Nayak KS. Unsolved problems and unmet needs: can MRI represent an accurate quantitative tool for assessing fat distribution in obesity research? In: Proceedings of the 16th Annual Meeting of ISMRM, Toronto, 2008.
26. Pineda AR, Reeder SB, Wen Z, Pelc NJ. Cramer-Rao bounds for three-point decomposition of water and fat. Magn Reson Med 2005; 54:625–635.
27. Brix G, Heiland S, Bellemann ME, Koch T, Lorenz WJ. MR imaging of fat-containing tissues: valuation of two quantitative imaging techniques in comparison with localized proton spectroscopy. Magn Reson Imaging 1993;11:977–991.
28. Deoni SC, Rutt BK, Peters TM. Rapid combined T1 and T2 mapping using gradient recalled acquisition in the steady state. Magn Reson Med 2003;49:515–526.
29. Johnson MS, Nagy TR. Animal body composition methods. In: Heymsfield SB, Lohman TG, Wang Z, Going SB, editors. Human body composition, 2nd edition. Champaign, IL: Human Kinetics Publishers; 2005. p 141–150.
30. Cunningham CH, Pauly JM, Nayak KS. Saturated double-angle method for rapid B1+ mapping. Magn Reson Med 2006;55:1326–1333.
31. Thomas LW. The chemical composition of adipose tissue of man and mice. Q J Exp Physiol Cogn Med Sci 1962;47:179–188.
32. Martin AD, Daniel MZ, Drinkwater DT, Clarys JP. Adipose tissue density, estimated adipose lipid fraction and whole body adiposity in male cadavers. Int J Obes Relat Metab Disord 1994;18:79–83.
33. Hu HH, Sung K, Nayak KS. Rapid proton density weighted abdominal MRI at 3 Tesla with RF non-uniformity correction. In: Proceedings of the 16th Annual Meeting of ISMRM, Toronto, 2008. (abstract 1249).
34. Franklin KM, Dale BM, Merkle EM. Improvement in B1-inhomogeneity artifacts in the abdomen at 3T MR imaging using a radiofrequency cushion. J Magn Reson Imaging 2008;27:1443–1447.
35. Murakami JW, Hayes CE, Weinberger E. Intensity correction of phased-array surface coil images. Magn Reson Med 1996;35:585–590.
36. Collins CM, Yang QX, Wang JH, et al. Different excitation and reception distributions with a single-loop transmit-receive surface coil near a head-sized spherical phantom at 300 MHz. Magn Reson Med 2002;47:1026–1028.
37. Wiesinger F, Sieifert F, Koenig H, Pruessmann KP. Unsolved problems and unmet needs: prospects of absolute B1 calibration. In: Proceedings of the 14th Annual Meeting of ISMRM, Seattle, 2006.
38. Goodpaster BH, Stenger VA, Boada F, et al. Skeletal muscle lipid concentration quantified by magnetic resonance imaging. Am J Clin Nutr 2004;79:748–754.
39. Machann J, Bachmann OP, Brechtel K, et al. Lipid content in the musculature of the lower leg assessed by fat selective MRI: intra- and interindividual differences and correlation with anthropometric and metabolic data. J Magn Reson Imaging 2003;17:350–357.
40. Reeder SB, Robson P, Yu H, et al. Quantification of hepatic steatosis with MRI: the effects of accurate fat spectral modeling. In: Proceedings of the 16th Annual Meeting of ISMRM, Toronto, 2008. (abstract 710).